

Knowledge Transfer in Deep Reinforcement Learning for Slice-Aware Mobility Robustness Optimization

Qi Liao*, Tianlun Hu*[†], Dan Wellington[‡]

*Nokia Bell Labs, Stuttgart, Germany

[†]Department of Informatics, Technical University of Munich, Germany

[‡]Nokia Software, Bellevue, United States

Email: qi.liao@nokia-bell-labs.com, {tianlun.hu, dan.wellington}@nokia.com

Abstract—The legacy mobility robustness optimization (MRO) in self-organizing networks aims at improving handover performance by optimizing cell-specific handover parameters. However, such solutions cannot satisfy the needs of next-generation network with network slicing, because it only guarantees the received signal strength but not the per-slice service quality. To provide the truly seamless mobility service, we propose a deep reinforcement learning-based slice-aware mobility robustness optimization (SAMRO) approach, which improves handover performance with per-slice service assurance by optimizing slice-specific handover parameters. Moreover, to allow safe and sample efficient online training, we develop a two-step transfer learning scheme: 1) regularized offline reinforcement learning, and 2) effective online fine-tuning with mixed experience replay. System-level simulations show that compared against the legacy MRO algorithms, SAMRO significantly improves slice-aware service continuation while optimizing the handover performance.

I. INTRODUCTION

The concept of self-organizing network (SON) was introduced nearly a decade ago when various use cases of SON were standardized by 3GPP [1]. However, the introduction of network slicing into 5G and beyond raises new challenges to SON, while the slice-aware SON has rarely been studied. Slice-aware SON requires solutions that satisfy the *slice-specific* service requirements, while the legacy SON solutions optimize *cell-specific* or *cell-pair-specific* (dedicated with respect to a neighboring cell) parameters by observing cell-specific Key Performance Indicators (KPIs).

In this paper, we study a particular use case of slice-aware SON, namely, the slice-aware mobility robustness optimization (SAMRO). The legacy MRO has the objective of minimizing the handover (HO)-related radio link failures (RLFs) and the number of unnecessary handovers. The decision variables are a set of cell-specific and cell-pair-specific HO parameters. The complexity and dynamics of user mobility result in a HO performance metric-related objective function that is in general non-convex, non-linear, and dependent on a high-dimensional HO parameter space. Thus, practical solutions include heuristics [2], reinforcement learning [3], and Bayesian methods [4]. However, these solutions, aiming to optimize the signal quality-based HO performance metrics, cannot guarantee the per-slice service continuation in terms of throughput and latency. A recent work [5] proposed to improve the quality of experience while optimizing the HO performance. However, with the cell-specific parameters, the HO optimization cannot be customized for every slice.

We propose a deep reinforcement learning (DRL)-based solution that provides a more seamless mobility service through the introduction of slice-specific HO parameters and performance metrics. Although the newly introduced parameters increase the dimensions of the state and action spaces, by utilizing model-free actor-critic architectures such as twin delayed deep deterministic policy gradient (TD3) [6], we can work with large continuous state and action spaces with significantly reduced model complexity, compared to the value-based algorithms such as deep Q-learning (DQN) [7].

Even with the help of the actor-critic architecture, we still face two challenges when developing a practical solution:

- *Large discrete action space*: In practical systems, HO parameters are selected from finite discrete sets, but directly working with huge discrete action space leads to intractable complexity. How to project the continuous agent actions to the discrete operating actions?
- *Effective training with knowledge transfer*: DRL approaches usually require substantial exploration, while in practice online training with unconstrained exploration is expensive. On the other hand, a large amount of biased data – usually collected in the safe operating space – is available. How to train more effectively by transferring knowledge from the biased offline data?

To overcome these challenges, we propose a two-step transfer learning-assisted SAMRO scheme, consisting of regularized offline DRL model training and online fine-tuning. The main contribution is threefold:

- *Mapping between continuous and discrete actions*: Motivated by [8], we use approximate nearest-neighbor methods to find the mapping between the continuous agent actions and the discrete operating actions.
- *Regularized offline DRL training*: We develop a regularized offline DRL algorithm to exploit the offline data, while dealing with the bias by regularizing the objective with the density estimates of state-action pairs.
- *Sample-efficient online fine-tuning*: We propose mixed experience replay during the online fine-tuning. The newly collected samples are mixed with a selected subset of offline samples for the batch training.

The rest of the paper is organized as follows. In Section II we define the system model and the slice-specific HO parameters and metrics. The SAMRO problem is discussed in Section III. Section IV introduces the proposed transfer learning and

actor-critic-based solution. The numerical results are shown in Section V. Section VI summarizes the conclusions.

II. SYSTEM MODEL

We consider a set of cells in the neighboring area, denoted by \mathcal{N} . Each cell can support numerous instances of different slices. Let the set of slices be denoted by \mathcal{S} . A service of slice $s \in \mathcal{S}$ has a defined throughput requirement η_s^* and latency requirement d_s^* . Assume that there are a set of B directional cell boundaries, denoted by $\mathcal{B} := \{(n_i, m_i) : n_i, m_i \in \mathcal{N}; i = 1, \dots, B\}$. In practice, if the boundary $(n, m) \in \mathcal{B}$, it means that cell m is within the neighboring cell list of cell n . Note that the boundary is directional, i.e., $(n, m) \neq (m, n)$ for $m \neq n$. Assume that if $(n, m) \in \mathcal{B}$, then $(m, n) \in \mathcal{B}$. Therefore, there are $B/2$ combinations (regardless of the order) of the neighboring cell-pairs. We denote the set of cell-pairs as \mathcal{B}' with $|\mathcal{B}'| = B/2$.

A. HO Process and Slice-Specific Parameters

In the legacy MRO, for any user served by cell $n \in \mathcal{N}$, a simplified HO criterion¹ for a handover from cell n to cell m when $(n, m) \in \mathcal{B}$ is that $P_m(t) > P_n(t) + O_{n,m}$ holds for a time duration of $T_{n,m}$, where P_m and P_n (in dBm) indicates the received signal strength from cell m and n respectively, and $O_{n,m}$ (in dB) and $T_{n,m}$ (in ms) are the handover margin (HOM) and time-to-trigger (TTT) from cell n to cell m .

The HOM and TTT defined above are on the cell-pair basis. We propose to define them also on the slice basis, such that the HO decision also considers whether the neighboring cell can provide the required service performance. The modified HO criterion for a service in slice s from cell n to cell m at time t' (in ms) is given by

$$P_m(t) > P_n(t) + O_{n,m,s}, \quad \forall t \in [t' - T_{n,m,s} + 1, t']. \quad (1)$$

Note that without loss of generality, (1) can be generalized to mobility-specific or even user-specific HO criteria. For example, we can group the users based on both mobility and slice classes, and define the user group-specific HO parameters. Since mobility-specific handover has been well studied [10], in this paper we focus on the slice-specific aspect to ensure the service continuation.

B. Slice-Specific HO Performance Metrics

The conventional HO optimization aims to reduce the following four HO events:

- *Too-late-handover (HOL)*: When a user is leaving the coverage area of its serving cell n towards the target cell m , but the handover is triggered too late which causes RLF before completing a handover.
- *Too-early-handover (HOE)*: This occurs when the HO decision is made too early. The neighboring cell cannot provide a sustainable signal quality to the user and a RLF happens right after the handover.
- *Wrong-cell-handover (HOW)*: This happens when the user is handed over to a wrong cell. A RLF is detected shortly after a successful handover to the target cell and then the user is connected to another neighboring cell.
- *Ping-pong-handover (HOPP)*: When a user is handed over from cell n to cell m , but after a short time period the handover from cell m back to cell n triggers.

¹The complete version can be found in [9, Section 5.5.4.4], but many offsets are not needed for intra-frequency handover.

A HO attempt can either fail or succeed. The handover failures includes HOL, HOE and HOW since they all cause RLFs, while the successful handovers includes HOPPs, although they cause unnecessary handovers. Let the counts of HO attempts, successful HOs, HOLs, HOEs, HOWs, and HOPPs for slice s and boundary (n, m) be denoted by $N_{n,m,s}^{(\text{HOA})}, N_{n,m,s}^{(\text{HOS})}, N_{n,m,s}^{(\text{HOL})}, N_{n,m,s}^{(\text{HOE})}, N_{n,m,s}^{(\text{HOW})}, N_{n,m,s}^{(\text{HOPP})}$, respectively. We propose to include them in the KPI reports for each slice $s \in \mathcal{S}$ and each boundary $(n, m) \in \mathcal{B}$.

We define the following two per-slice **HO metrics to minimize**, *handover failure ratio (HFR)* and *ping-pong ratio (PPR)*:

$$R_s^{(\text{HF})} = \frac{\sum_{(n,m) \in \mathcal{B}} N_{n,m,s}^{(\text{HOL})} + N_{n,m,s}^{(\text{HOE})} + N_{n,m,s}^{(\text{HOW})}}{\sum_{(n,m) \in \mathcal{B}} N_{n,m,s}^{(\text{HOA})}} \quad (2)$$

$$R_s^{(\text{PP})} = \frac{\sum_{(n,m) \in \mathcal{B}} N_{n,m,s}^{(\text{HOPP})}}{\sum_{(n,m) \in \mathcal{B}} N_{n,m,s}^{(\text{HOS})}}. \quad (3)$$

Since $N_{n,m,s}^{(\text{HOA})} = N_{n,m,s}^{(\text{HOS})} + N_{n,m,s}^{(\text{HOL})} + N_{n,m,s}^{(\text{HOE})} + N_{n,m,s}^{(\text{HOW})}$ and $N_{n,m,s}^{(\text{HOPP})} \leq N_{n,m,s}^{(\text{HOS})}$, we have $R_s^{(\text{HF})} \in [0, 1]$ and $R_s^{(\text{PP})} \in [0, 1], \forall s \in \mathcal{S}$.

C. Slice-Specific Service Quality Metrics

As reflected in (1), the above-introduced HO metrics are signal quality based. To observe the per-slice service performance, we define in below two **service metrics to maximize**, *throughput service level (TSL)* $L_{k,s}^{(\text{T})}$ and *latency service level (LSL)* $L_{k,s}^{(\text{D})}$ for each user k associated to slice $s \in \mathcal{S}$:

$$L_{k,s}^{(\text{T})} = \min \left\{ \frac{\eta_{k,s}}{\eta_s^*}, 1 \right\} \quad \text{and} \quad L_{k,s}^{(\text{D})} = \min \left\{ \frac{d_s^*}{d_{k,s}}, 1 \right\}, \quad (4)$$

where $\eta_{s,k}$ and $d_{s,k}$ are the achieved throughput and latency of user k associated to slice s , respectively. Note that $L_{s,k}^{(\text{T})}$ and $L_{s,k}^{(\text{D})}$ are upper bounded by 1. Thus, as long as the service quality is satisfied, we have $L_{s,k}^{(\text{T})} = L_{s,k}^{(\text{D})} = 1$.

Let the set of users associated to cell n and slice s be denoted by $\mathcal{K}_{n,s}$ with the cardinality $|\mathcal{K}_{n,s}| = K_{n,s}$. Let each cell n report to the central agent the following three measures: 1) number of the users in each slice $K_{n,s}$, 2) the per-slice sum TSL $L_{n,s}^{(\text{T})} := \sum_{k \in \mathcal{K}_{n,s}} L_{k,s}^{(\text{T})}$, and 3) the per-slice sum LSL $L_{n,s}^{(\text{D})} := \sum_{k \in \mathcal{K}_{n,s}} L_{k,s}^{(\text{D})}$. The slice-specific average TSL and LSL for the considered area is given by

$$L_s^{(\text{T})} = \frac{\sum_{n \in \mathcal{N}} L_{n,s}^{(\text{T})}}{\sum_{n \in \mathcal{N}} K_{n,s}} \quad \text{and} \quad L_s^{(\text{D})} = \frac{\sum_{n \in \mathcal{N}} L_{n,s}^{(\text{D})}}{\sum_{n \in \mathcal{N}} K_{n,s}}. \quad (5)$$

With (4), we have $L_s^{(\text{T})} \in [0, 1]$ and $L_s^{(\text{D})} \in [0, 1], \forall s \in \mathcal{S}$.

D. Markov Decision Process Model

We model the multi-cell system as a Markov decision process (MDP), defined by the tuple $(\mathcal{S}, \mathcal{A}, P(\cdot), r(\cdot), \gamma)$, where $P : \mathcal{S} \times \mathcal{A} \times \mathcal{S} \rightarrow [0, 1]$ indicates the transition dynamics by a conditional distribution over the state space \mathcal{S} and the action space \mathcal{A} , $r : \mathcal{S} \times \mathcal{A} \rightarrow \mathbb{R}$ denotes the reward function, and $\gamma \in [0, 1]$ is the discount factor. We define the action, state, and reward of the MDP as follows.

1) *Action*: Assume HOM $O_{n,m,s} \in \mathcal{O}$ and TTT $T_{n,m,s} \in \mathcal{T}$, where \mathcal{O} and \mathcal{T} are in practice both finite discrete sets. The $2BS$ -dimensional action $\mathbf{a} \in \mathcal{A}$ is defined as

$$\mathbf{a} := [(O_{n,m,s}, T_{n,m,s}) : O_{n,m,s} \in \mathcal{O}, T_{n,m,s} \in \mathcal{T}, (n, m) \in \mathcal{B}, s \in \mathcal{S}] \in \mathcal{A} := (\mathcal{O} \times \mathcal{T})^{BS}. \quad (6)$$

TABLE I: Measures included in the state

Per-cell per-slice states	Per-cell-pair per-slice states
$\forall n \in \mathcal{N}, s \in \mathcal{S} :$ · Load $l_{n,s}$ · Number of users $K_{n,s}$ · TSL $L_{n,s}^{(T)}$ · LSL $L_{n,s}^{(D)}$	$\forall (n, m) \in \mathcal{B}', s \in \mathcal{S} :$ · HO attempts $N_{n,m,s}^{(\text{HOA})} + N_{m,n,s}^{(\text{HOA})}$ · Successful HOs $N_{n,m,s}^{(\text{HOS})} + N_{m,n,s}^{(\text{HOS})}$ · HOLs $N_{n,m,s}^{(\text{HOL})} + N_{m,n,s}^{(\text{HOL})}$ · HOPPs $N_{n,m,s}^{(\text{HOPP})} + N_{m,n,s}^{(\text{HOPP})}$

2) *State*: As shown in Table I, the network state $\mathbf{s} \in \mathbb{R}^{(4N+2B)S}$ includes $4NS$ per-cell per-slice measurements and $2BS$ per-cell-pair per slice HO event counts (with $B/2$ cell-pairs, we have $4 * (B/2) * S = 2BS$ per-cell-pair per-slice states). Note that we use the counts of HO events directly instead of HFR and PPR defined in Section II-B because of two reasons: 1) sometimes the number of HO attempts is zero and using raw counts avoids zero denominators, and 2) raw counts may provide more information reflecting too-early and too-late HO decisions. Also, we reduce the dimension of state by adding the HO event counts of the both directions of the cell boundaries. For the same reason we do not include the counts of HOE and HOW into the state, since we expect that the count of HOPPs indicates the too-early HO decisions.

3) *Reward*: The reward function is a utility function based on the HO metrics $R_s^{(\text{HF})}$ and $R_s^{(\text{PP})}$ defined in (2) and (3) respectively, and the service metrics $L_s^{(\text{T})}$ and $L_s^{(\text{D})}$, for $s \in \mathcal{S}$ defined in (5). For example, one option is given by:

$$r = \sum_{s \in \mathcal{S}, X \in \{\text{T}, \text{D}\}} w_s^{(X)} L_s^{(X)} - \sum_{s \in \mathcal{S}, X \in \{\text{HF}, \text{PP}\}} w_s^{(X)} R_s^{(X)}. \quad (7)$$

where $w_s^{(X)}$ for $s \in \mathcal{S}$, $X \in \{\text{T}, \text{D}, \text{HF}, \text{PP}\}$ are the weight factors. Note that $L_s^{(\text{D})}$ is the latency satisfaction level that is **inversely** proportional to latency – a larger value indicates higher satisfaction by meeting the latency constraints (4). The designed reward function incentives to improve the service quality satisfaction level, as well as to minimize the handover failures and unnecessary handovers. Because all the metrics included in reward are within $[0, 1]$, we have the same scale for the metrics, and the reward is bounded.

III. PROBLEM STATEMENT

As many classical reinforcement learning problems, we want to find a policy $\pi : \mathcal{S} \rightarrow \mathcal{A}$ which decides the HO parameters \mathbf{a}_t based on the network state \mathbf{s}_t , to maximize the expectation of the cumulative discounted reward of a finite horizon H :

$$\underset{\pi}{\text{maximize}} \mathbb{E}_{\pi} \left[\sum_{t=0}^H \gamma^t r(\mathbf{s}_t, \mathbf{a}_t) \right], \text{ s.t. } \mathbf{a} \in \mathcal{A}. \quad (8)$$

However, we face the following two challenges. The first one is the complexity caused by the enormous discrete action space. In 3GPP, it is defined $\mathcal{O} := \{-24, -23, \dots, 23, 24\}$ (in dB) and $\mathcal{T} := \{0, 40, 64, 80, 100, 128, 160, 256, 320, 480, 512, 640, 1024, 1280, 2560, 5120\}$ (in ms) [9], which means $|\mathcal{O}| = 49$ and $|\mathcal{T}| = 16$. Even for a neighboring area of 9 cells, assuming that each cell only has 2 neighboring cells, we have 36 directional cell boundaries. With only 2 slices per cell, the size of the action space yields $|\mathcal{A}| = (49 * 16)^{72} > 1e208$. This is intractable with the value-approximation methods for discrete action space such as DQN.

The second challenge is raised by the high cost of online interaction. Reinforcement learning, especially with large state and action spaces, usually requires sufficient exploration to converge. However, in real-world network systems, executing actions leading to unknown states may trigger risky network states. On the other hand, it is possible to collect an off-policy sample set $\{(\mathbf{s}_t, \mathbf{a}_t, \mathbf{s}_{t+1}, r_t) : t \in \mathbb{N}_0\}$ in the safe operating action space. Thus, our problem is to learn from a biased offline sample set with a minimal number of online interactions.

IV. PROPOSED APPROACH

To deal with the large discrete action space, we propose a policy built upon the actor-critic algorithms with a projection policy that maps the continuous proto-action to its nearest neighbors in the discrete action space \mathcal{A} . We describe TD3 [6] as the applied actor-critic algorithm in Section IV-A. Then, we propose the action projection policy in Section IV-B. To learn from the biased data, we propose in Section IV-C a transfer learning approach for DRL that comprises two steps: 1) regularized offline DRL, and 2) online DRL model fine-tuning.

A. Actor-Critic Algorithm

The objective function in (8) can be seen as a state-action value function $Q^{\pi}(\mathbf{s}, \mathbf{a}) = \mathbb{E}^{\pi} \left[\sum_{t=0}^H \gamma^t r_t | \mathbf{s}_0 = \mathbf{s}, \mathbf{a}_0 = \mathbf{a} \right]$. The value function Q^{π} can be expressed in a recursive manner using the Bellman equation [11]:

$$Q^{\pi}(\mathbf{s}, \mathbf{a}) = r(\mathbf{s}, \mathbf{a}) + \gamma \sum_{\mathbf{s}' | \mathbf{s}, \mathbf{a}} Q^{\pi}(\mathbf{s}', \pi(\mathbf{s}')). \quad (9)$$

For value-based DRL in discrete space, $Q^{\pi}(\mathbf{s}, \mathbf{a})$ is approximated by a neural network which takes both state and action as input, and output $|\mathcal{A}|$ evaluations of Q values corresponding to every possible action. Then, it chooses the action with the best estimation of the Q value to execute. Unfortunately, because its complexity grows linearly with $|\mathcal{A}|$, it is intractable when the discrete action space is huge.

We consider next relaxing the action space to the continuous space, which enables us to apply the actor-critic method in the continuous action space. More details of action projection will be provided in Section IV-B.

The actor-critic method solves the optimization problem by using a critic $Q_{\theta}(\mathbf{s}_t, \mathbf{a}_t)$ to approximate the value function, i.e., $Q_{\theta}(\mathbf{s}_t, \mathbf{a}_t) \approx Q^{\pi}(\mathbf{s}_t, \mathbf{a}_t)$ and an actor $\pi_{\omega}(\mathbf{s}_t)$ to update the policy π at every step in the direction suggested by critic. The critic and actor both modeled with neural networks are characterized by parameters θ and ω , respectively. In this way, unlike DQN having $|\mathcal{A}| = (|\mathcal{O}||\mathcal{T}|)^{BS}$ outputs for our problem formulation (it estimates Q values corresponding to all possible actions), the actor has an output dimension of $2BS$ because it directly predicts the action $\mathbf{a} \in \mathbb{R}^{2BS}$.

We follow a particular actor-critic algorithm, namely, the TD3 [6], to train the agents, which has proven effectiveness when dealing with high dimensional and continuous state space. As an extension of deep deterministic policy gradient (DDPG) [12], TD3 overcomes the DDPG's problem of overestimating Q values by introducing double critic structure for both current networks $Q_{\theta_1}, Q_{\theta_2}$ and target networks $Q_{\theta'_1}, Q_{\theta'_2}$. The minimum of the two Q values is used to represent the approximated Q value of the next state. Moreover, TD3 uses smoothing for target policy $\pi_{\omega'}$, i.e., adding noise to

the target action to make it harder for the policy to exploit Q-function errors by smoothing out Q along changes in action. The target actions are computed by

$$\mathbf{a}'(\mathbf{s}_{t+1}) = \text{clip}(\pi_{\omega'}(\mathbf{s}_{t+1}) + \text{clip}(\epsilon, -c, c), \mathbf{a}_L, \mathbf{a}_H), \quad (10)$$

where the added noise $\epsilon \sim \mathbb{N}(0, \sigma)$ is clipped within $[-c, c]$ to keep the target close to the original action, and $\mathbf{a}_L, \mathbf{a}_H$ are the lower and upper bounds of the action, respectively.

The critics' parameters $\theta_i, i = 1, 2$ are updated with temporal difference (TD) learning, given by:

$$L(\theta_i) = \mathbb{E} \left[(y_t - Q_{\theta_i}(\mathbf{s}_t, \mathbf{a}_t))^2 \right], i = 1, 2 \quad (11)$$

$$\text{where } y_t = r_t + \gamma \min_{i=1,2} Q_{\theta_i}'(\mathbf{s}_{t+1}, \mathbf{a}'(\mathbf{s}_{t+1})).$$

The actor is updated with the policy gradient on the expected accumulated regularized reward, give by

$$\mathbb{E} \left[\nabla_{\mathbf{a}} Q_{\theta_1}(\mathbf{s}, \mathbf{a}) \Big|_{\mathbf{s}=\mathbf{s}_t, \mathbf{a}=\pi_{\omega}(\mathbf{s}_t)} \nabla_{\omega} \pi_{\omega}(\mathbf{s}) \Big|_{\mathbf{s}=\mathbf{s}_t} \right]. \quad (12)$$

B. Dealing with Large Discrete Action Space

In this part, we propose the method to relax the discrete action space to the continuous space, as well as to map the proto-action back to the discrete action by approximating its nearest neighbors in \mathcal{A} .

Motivated by [8], given the proto-action $\tilde{\mathbf{a}}$ as the output of actor $\pi : \mathcal{S} \rightarrow \mathbb{R}^{2BS}$, it is very likely that $\tilde{\mathbf{a}} \notin \mathcal{A}$. We need to design a policy to map $\tilde{\mathbf{a}}$ to an action in the desired discrete space $\hat{\mathbf{a}} \in \mathcal{A}$. The mapping policy is similar to the *Wolpertinger Policy* in [8], summarized in Algorithm 1. We first find with policy G_k (Algorithm 2) the k nearest neighbors of $\tilde{\mathbf{a}}$ in \mathcal{A} , denotes by $\mathcal{A}_k(\tilde{\mathbf{a}}) := \{\mathbf{a}^{(1)}, \dots, \mathbf{a}^{(k)}\}$, then select the one with the best Q-estimates (estimated by the critic function) as the action applied to the environment. The mapped $\hat{\mathbf{a}} \in \mathcal{A}$ is given by:

$$\hat{\mathbf{a}} = \arg \max_{\mathbf{a} \in G_k \circ \pi_{\omega}(\tilde{\mathbf{a}})} Q_{\theta_1}(\mathbf{s}, \mathbf{a}). \quad (13)$$

As for the strategies of selecting k nearest neighbors

Algorithm 1 Action Projection Policy

- 1: Get state \mathbf{s}
 - 2: $\tilde{\mathbf{a}} = \pi_{\omega}(\mathbf{s})$ ▷ Get proto-action from actor
 - 3: $\mathcal{A}_k(\tilde{\mathbf{a}}) = G_k(\tilde{\mathbf{a}})$ ▷ Get k nearest neighbors of $\tilde{\mathbf{a}}$
 - 4: $\hat{\mathbf{a}} = \arg \max_{\mathbf{a} \in \mathcal{A}_k(\tilde{\mathbf{a}})} Q_{\theta_1}(\mathbf{s}, \mathbf{a})$
 - 5: Apply $\hat{\mathbf{a}}$ to environment; receive r, \mathbf{s}' .
-

$G_k : \mathbb{R}^{2BS} \rightarrow \mathcal{A}^k$, in [8] the authors use approximate nearest neighbor methods based on K-Means tree structure [13] allowing for logarithmic-time search complexity relative to the size of action space $O(ZBS(\log |\mathcal{A}| / \log k))$, where Z is the maximum number of points to examine (a hyperparameter of the algorithm). However, except for the search complexity, the tree construction complexity is also substantially high and requires extra large memory space. Considering that our action space is already well structured (containing gridded points in high-dimensional space), we propose a coarse, heuristic, but more efficient way to approximate the k neighbors with the search complexity $O(kBS(|\mathcal{O}| + |\mathcal{T}|))$, described in Algorithm 2. Let the j -th dimension of $\tilde{\mathbf{a}}$ be denoted by \tilde{a}_j . The intuition is to choose the nearest values in \mathcal{O} or \mathcal{T} along each dimension with the probability depending on the reciprocal of the distance from $\tilde{a}_j, \forall j$. The proposed heuristics can quickly generate k neighbors of $\tilde{\mathbf{a}}$ in \mathcal{A} .

Algorithm 2 Approximate k neighbor selection

- 1: $\mathcal{A}_k(\tilde{\mathbf{a}}) \leftarrow \emptyset$
 - 2: **for** the i -th neighbor to be generated, $i \in \{1, \dots, k\}$ **do**
 - 3: **for** $j \in \{1, \dots, 2BS\}$ **do**
 - 4: $\Omega \leftarrow \mathcal{O}$ if the dimension is HOM, o/w $\Omega \leftarrow \mathcal{T}$
 - 5: **if** $\tilde{a}_j \geq \max(\Omega)$ or $\tilde{a}_j \leq \min(\Omega)$ **then**
 - 6: $a_j^{(i)} \leftarrow \arg \min_{x \in \Omega} |x - \tilde{a}_j|$
 - 7: **else**
 - 8: $a_j^+ \leftarrow \arg \min_{x \in \Omega, x \geq \tilde{a}_j} |x - \tilde{a}_j|$
 - 9: $\nu_j^+ \leftarrow 1 / (a_j^+ - \tilde{a}_j)$
 - 10: $a_j^- \leftarrow \arg \min_{x \in \Omega, x \leq \tilde{a}_j} |x - \tilde{a}_j|$
 - 11: $\nu_j^- \leftarrow 1 / (\tilde{a}_j - a_j^-)$
 - 12: $p_j^+ \leftarrow \nu_j^+ / (\nu_j^+ + \nu_j^-); p_j^- \leftarrow 1 - p_j^+$
 - 13: $\Pr \left\{ a_j^{(k)} \leftarrow a_j^+ \right\} = p_j^+$ and
 - 14: $\Pr \left\{ a_j^{(k)} \leftarrow a_j^- \right\} = p_j^-$
 - 15: $\mathbf{a}^{(i)} \leftarrow [a_1^{(i)}, \dots, a_{2BS}^{(i)}]$
 - 16: $\mathcal{A}_k(\tilde{\mathbf{a}}) \leftarrow \mathcal{A}_k(\tilde{\mathbf{a}}) \cup \{\mathbf{a}^{(i)}\}$
-

C. Transfer Learning in Deep Reinforcement Learning

The proposed transfer learning approach comprises of two steps: 1) regularized offline actor-critic training, and 2) online fine-tuning with mixed replay buffer sampling.

1) Regularized Offline Deep Reinforcement Learning:

Off-policy batch reinforcement learning [14] performs the task of learning from a collected dataset $\mathcal{D} := \{(\mathbf{s}^{(i)}, \mathbf{a}^{(i)}, \mathbf{s}'^{(i)}, r^{(i)}) : i = 1, \dots, D\}$ without further interactions with the environment. In the Telecom industries, however, the available data usually contains network configurations in a safe operating space. Such biased dataset causes the algorithms to fail because of a fundamental problem of *extrapolation error*, a phenomenon in which the model erroneously over-estimates the Q values of the unseen state-action pairs, and outputs the actions with over-estimated unrealistic rewards (see Fig. 3). To overcome the challenge, we propose to add a regularization term to the reward function, such that the probability of the state-action pair is also maximized. Note that this motivation is opposite to some of the online algorithms that encourage the exploration by maximizing the expected entropy of the policy. The rationale is that, for the offline optimization without interaction with the environment, exploring outside of training data distribution leads to unrealistic over-estimated values.

We replace the reward r in (8) and (9) by

$$r'(\mathbf{s}_t, \mathbf{a}_t) = r(\mathbf{s}_t, \mathbf{a}_t) + \alpha \log p(\mathbf{s}_t, \mathbf{a}_t), \quad (14)$$

where $p(\mathbf{s}_t, \mathbf{a}_t)$ is the probability density function that $(\mathbf{s}_t, \mathbf{a}_t)$ appears in the training dataset, and α is a weight factor. The remaining problem is how to compute the log-density estimation $\log p(\mathbf{s}_t, \mathbf{a}_t)$. Density estimation for complex high-dimensional data is a challenging fundamental problem in statistical learning. Assuming that we observe a random vector $\mathbf{x} \in \mathbb{R}^d$ and want to use a parametrized density model to approximate the log-density function $\log p_{\mathbf{x}}(\cdot)$. An efficient method is the energy-based models, i.e., to define an energy function $\mathcal{E}_{\mathbf{x}}(\cdot)$ which is essentially an unnormalized log-density function for the given data, and define the score function $\phi(\mathbf{x}) = \nabla_{\mathbf{x}} \log p_{\mathbf{x}}(\mathbf{x}) = -\nabla_{\mathbf{x}} \mathcal{E}_{\mathbf{x}}(\mathbf{x})$. The energy function can be then estimated using *score matching* [15]. In this work, we apply a promising denoising score matching-based solution, deep energy estimator network (DEEN),

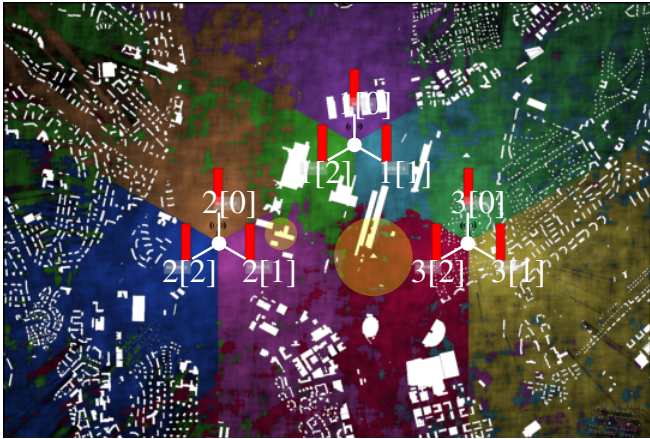


Fig. 1: The 9-cell simulation environment. Red bar indicates the cell throughput at the snapshot. White areas are the buildings. Yellow circles define the mobility areas of the hotspots.

which uses a neural network to model the energy $\mathcal{E}_\psi(\mathbf{x})$ characterized by parameters ψ . Due to the limited space, we do not give full details but refer the interested readers to [16]. The regularized reward in (14) is then given by

$$r'(s_t, \mathbf{a}_t | \psi) = r(s_t, \mathbf{a}_t) - \alpha \mathcal{E}_\psi(s_t, \mathbf{a}_t) \quad (15)$$

It is also worth noting that the size of the offline dataset \mathcal{D} is limited, and the collected operating actions are discrete. To fully exploit them to train the offline DRL whose outputs of actor are continuous, we can use the inverse policy of the neighbor selection strategy in Algorithm 2 for the data augmentation of the training set. Similar to generating the discrete neighbors of a proto-action, we generate the k neighboring continuous actions $\tilde{\mathcal{A}}_k(\mathbf{a}) := \{\tilde{\mathbf{a}}^{(i)} : i = 1, \dots, k\}$ near the discrete action in the dataset $\mathbf{a} \in \mathcal{A}$. In this way, from each sample $(s, \mathbf{a}, s', r) \in \mathcal{D}$, we augment k samples with actions in the continuous space $\{(s, \tilde{\mathbf{a}}, s', r) : \forall \tilde{\mathbf{a}} \in \tilde{\mathcal{A}}_k(\mathbf{a})\}$, and the training dataset is extended to $\bar{\mathcal{D}}$ with size kD .

2) *The Online Fine-tuning of the Pretrained Models:* We expect that the offline pretrained actor-critic agent provides us a good initialization of the online operation. However, to adapt to the real-time system that may have a distribution drift from the training data, we allow the model to fine-tune itself with the real-time interaction with the environment. To this end, we propose to build two replay buffers: $B^{(\text{off})}$ stores offline training data, while $B^{(\text{on})}$ stores the updated new samples. For each training update of the online agent, the mini-batch can be sampled from either $B^{(\text{off})}$ or $B^{(\text{on})}$. During the training, we gradually decrease the probability of sampling from $B^{(\text{off})}$, while increase the probability of sampling from $B^{(\text{on})}$. Meanwhile, along with the actor and critic networks, we also periodically update the energy estimation network $\mathcal{E}_\psi(\mathbf{x})$ based on the updated offline and online datasets. The TD3-based SAMRO algorithm is then provided in Algorithm 3. Note that TD3 builds two critic networks and takes the minimum value between them to limit the over-estimation of the Q value.

V. NUMERICAL RESULTS

We test the SAMRO algorithm proposed in Section IV with a realistic system-level SON simulator, as an extension with network slicing of the emulator in [17].

1) *Simulator Scenario:* We consider an environment with 3 three-sector sites, i.e., 9 cells, operating on the frequency band 2.4 GHz, as shown in Fig. 1. The radio propagation

Algorithm 3 TD3-based SAMRO with knowledge transfer

1: **Initialize:**

Critic networks $Q_{\theta_i}, i = 1, 2$

Actor network π_ω

Target critic networks $Q_{\theta'_i}, i = 1, 2$

Target actor network $\pi_{\omega'}$

Energy estimator network \mathcal{E}_ψ

Replay buffers $B^{(\text{off})} \neq \emptyset$ and $B^{(\text{on})} \leftarrow \emptyset$

Buffer prioritization factor β

2: **for** $t = 1, \dots, T$ **do**

3: Output action with exploration noise $\tilde{\mathbf{a}} \leftarrow \pi_\omega(\mathbf{s}) + \epsilon$

4: Select operating action $\hat{\mathbf{a}}$ using Algorithm 1

5: Observe r and new state s'

6: Store transition tuple $(s, \tilde{\mathbf{a}}, s', r)$ in $B^{(\text{on})}$

7: Sample mini-batch of M transitions from $B^{(\text{on})}$ with probability β while from $B^{(\text{off})}$ with probability $1 - \beta$

8: $\tilde{\mathbf{a}}' \leftarrow \pi_{\omega'}(s')$

9: Update r' with (15)

10: $y \leftarrow r' + \gamma \min_{i=1,2} Q_{\theta'_i}(s', \tilde{\mathbf{a}}')$

11: Update critics' weights $\theta_i, i = 1, 2$ by minimizing the sampled loss of (11)

12: **if** $t \bmod H^{(A)}$ **then**

13: Update actor weights ω using the sampled

14: gradient of (12) and update the target networks'

15: weights $\theta'_i, i = 1, 2$ and ω'

16: **if** $t \bmod H^{(E)}$ **then**

17: Update energy estimator network weights ψ

18: Update β

TABLE II: User Groups

	Group size	Traffic Type	Expected Rate	Speed
Group 1	25	Slice 1 (Video)	5 Mbit/s	6 km/h
Group 2	25	Slice 2 (HTTP)	3 Mbit/s	3 km/h
Hotspot 1	8	Slice 1 (Video)	5 Mbit/s	3 km/h
Hotspot 2	8	Slice 1 (Video)	5 Mbit/s	3 km/h

model is Winner+ [18] supported with ray tracing. In Table II, we define four groups of users associated to two slices: "Slice 1" supporting video traffic and "Slice 2" supporting HTTP traffic. The users in groups 1 and 2 move uniformly randomly within the playground and those in hotspots move within the circled areas as shown in Fig. 1. Due to the limitation of the scheduler in simulator, we assume all slices have the same latency requirement of 1 ms but different throughput requirements. We also generate a realistic traffic pattern to each of the user group as shown in Fig. 2. The agent interacts with the simulator with a time granularity of 900 simulation slots, which reflects 15-min of the real-life time. Namely, a one-day operation (in simulator) allows 96 interactions with the simulated environment.

2) *Offline Regularized Deep Reinforcement Learning:* Following the state and action defined in Section II-D, we define $N = 9$, $S = 2$, and $B = 34$. Thus, the state $\mathbf{s} \in \mathbb{R}^{208}$ and the proto-action $\tilde{\mathbf{a}} \in \mathbb{R}^{136}$. We define $\mathcal{O} := \{-5, -4, \dots, 5\}$ in dB and $\mathcal{T} := \{40, 64, 80, 100, 128, 160, 256, 320, 480, 512, 640, 1024, 1280, 2560, 5120\}$ in ms. Thus, we also define the upper and lower bounds for each dimension of the proto-action. We assume that in practice the default value of HOM is 0 dB and TTT is 512 ms. We have collected 20,000 offline biased samples as follows. Firstly, we generated independent normal distributed r.v.s for each dimension of $\tilde{\mathbf{a}}$ with the mean as the default value, and the variance of 3 dB for HOM and 300 ms for TTT, respectively. Then, we find the

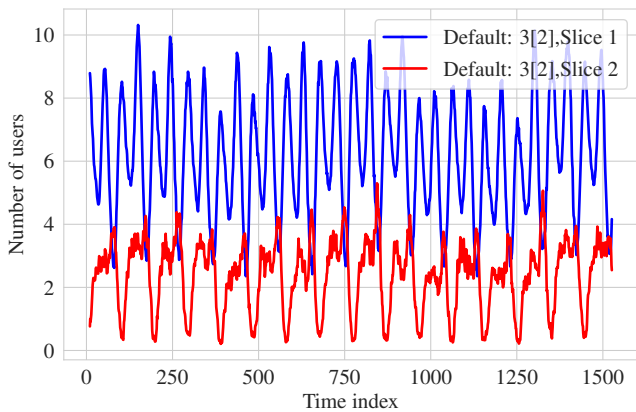


Fig. 2: Number of connected users in Cell “3[2]” with hotspot when HO parameters are set to default.

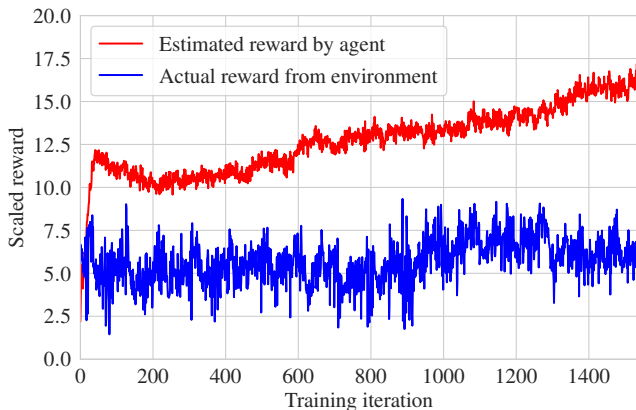


Fig. 3: Phenomenon of extrapolation error.

nearest value in \mathcal{O} or \mathcal{T} and send the discrete action back to the simulator. The reward weights $w_s^{(T)}$, $w_s^{(D)}$, $w_s^{(HF)}$, $w_s^{(PP)}$ are set as 1, 1, 1, 0.3, respectively. It is worth noting that sometimes scaling the reward values help improve the convergence. We scale the reward with a factor of 5. With the defined weights, after the scaling the range of the reward is $[-6.5, 10]$. We choose small discount $\gamma = 0.1$ because optimizing the network configuration for every 15-min mainly influences the instantaneous reward.

As for the actor-critic networks, we use multi-layer perception (MLP) for the actor and critic networks, both with 3 hidden layers, and numbers of neurons for each layer are (128, 64, 32) and (64, 16, 4), respectively. Learning rates of the actor and critic are 0.001 and 0.002, respectively. The batch size is 64, and the optimizer is Adam. For the DEEN, we also use 3 layers with the sizes (256, 64, 32). The batch size is 32 and the noise scale is 0.1. The update periods of actor and DEEN are $H^{(A)} = 3$ and $H^{(E)} = 100$ respectively.

Fig. 3 illustrates a typical extrapolation error when we train an offline DRL without regularization in Fig. 3. To verify this, we set the discount factor $\gamma = 0$ such that the critic simply predicts the instantaneous reward and the policy should output the action with the best reward. However, after 30 mini-batches, the agent starts over-estimating the reward for unseen actions (even exceed the upper-bound).

Fig. 4 shows the training loss functions of the actor and critics with the regularization. The regularized term help the negative actor loss (reflecting the Q estimate of the chosen next action) to be well bounded within the scaled reward region and prevent from outputting an action outside of the training data distribution.

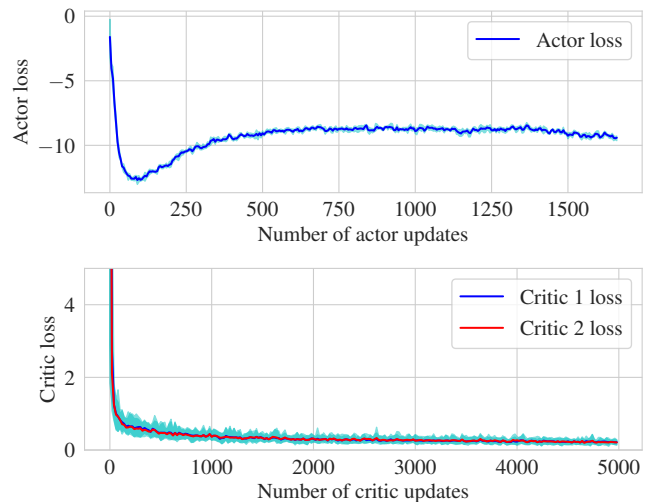


Fig. 4: Training loss of actor and critic networks.

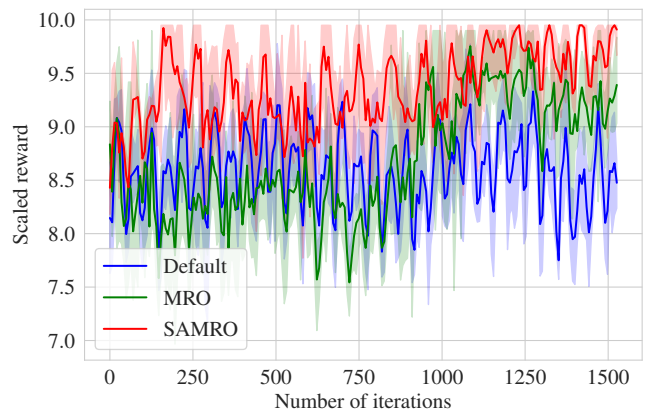


Fig. 5: Online training against baselines.

3) *TD3-Based SAMRO with Knowledge Transfer*: To show the advantage introduced by slice-specific HO parameters and KPIs, we compare our SAMRO approach with two baselines: 1) MRO optimized with the same DRL with transfer learning approach, but without slice-awareness, and 2) default setting of HOM to be 0 dB and TTT to be 512 ms.

Fig. 5 shows that our approach helps both SAMRO and MRO converge faster and outperform the default setting with both higher start and higher asymptote, when assuming only two weeks of online training (1344 training interactions) and two days of testing (192 testing interactions).

Fig. 6 illustrates the empirical cumulative density functions (CDFs) of *HO metrics HO failure ratio* and *ping-long HO ratio* and the slice service metrics *throughput service level* and *latency service level*, respectively. We observe that SAMRO further outperforms MRO because it not only improves the HO performance, but also reduces the violation of the throughput and latency constraints of each slice. For example, SAMRO guarantees that more than 55% and 70% of the services satisfy the throughput requirements of Slice 1 and 2, respectively, while MRO satisfies only less than 20% and 40%, respectively. Moreover, SAMRO achieves a good tradeoff between the too-late and too-early HO metrics. It significantly reduces the too-early HO events (e.g., ping-pong HOs), without increasing the HO failures.

VI. CONCLUSIONS

In this paper, we proposed a novel SAMRO solution with the newly introduced slice-specific HO parameters and KPIs,

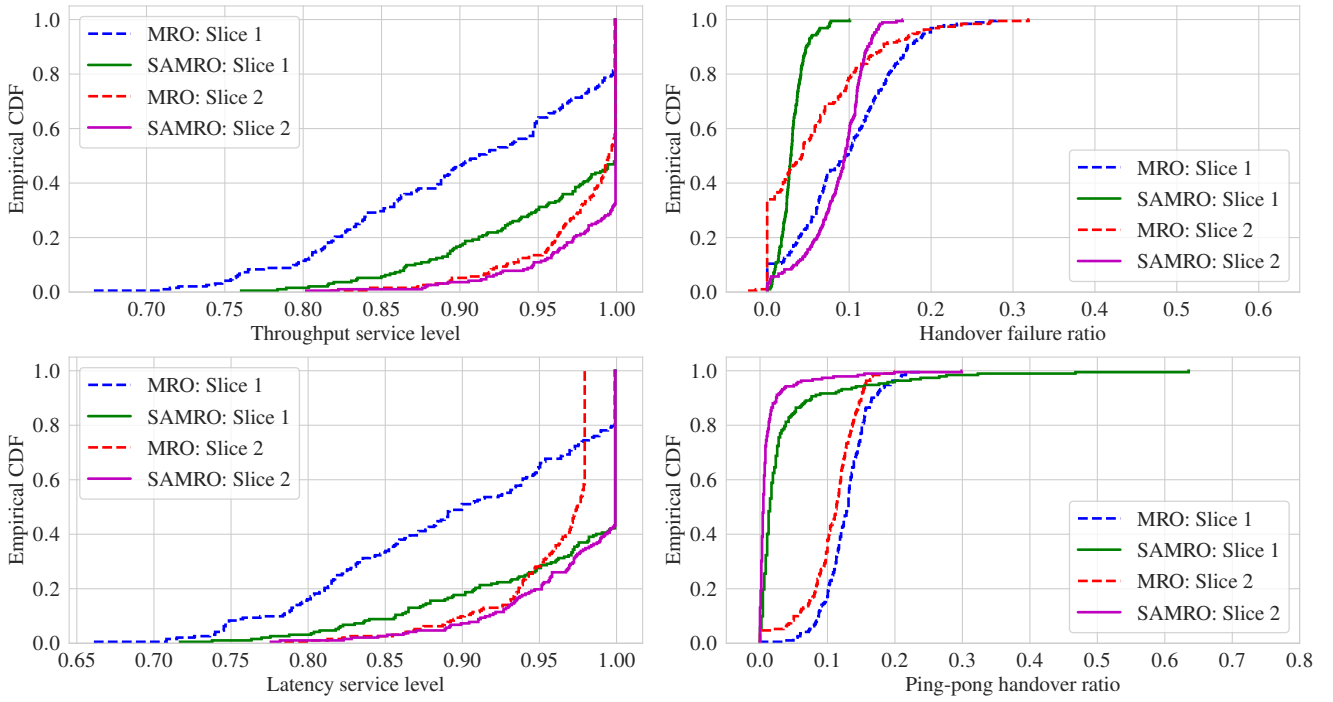


Fig. 6: Comparison of the service and HO quality.

optimizing both service quality and handover performance for diverse slices. We also proposed a two-step transfer learning-empowered actor-critic scheme that can deal with large discrete spaces, and enable safe and effective online training with regularized objective function and mixed replay buffer sampling. The system-level simulation shows significant performance benefits versus the baseline algorithms without slice-awareness.

ACKNOWLEDGEMENT

The authors would like to thank Senthil Kumaran K and Niraj Nanavaty for providing the practical insights.

REFERENCES

- [1] "TS 32.500, Self-Organizing Networks (SON); Concepts and requirements, Rel-16," 3GPP, Technical Specification, 2020.
- [2] M. T. Nguyen, S. Kwon, and H. Kim, "Mobility robustness optimization for handover failure reduction in LTE small-cell networks," *IEEE Trans. on Vehicular Technology*, vol. 67, no. 5, pp. 4672–4676, 2017.
- [3] S. S. Mwanje and A. Mitschele-Thiel, "Distributed cooperative Q-learning for mobility-sensitive handover optimization in LTE SON," in *2014 IEEE ISCC*, 2014, pp. 1–6.
- [4] Q. Liao, S. Stańczak, and F. Penna, "A statistical algorithm for multi-objective handover optimization under uncertainties," in *IEEE WCNC*, 2013, pp. 1552–1557.
- [5] M. L. Marí-Altozano, S. S. Mwanje, S. L. Ramírez, M. Toril, H. Saneck, and C. Gijón, "A service-centric Q-learning algorithm for mobility robustness optimization in LTE," *IEEE Transactions on Network and Service Management*, vol. 18, no. 3, pp. 3541–3555, 2021.
- [6] S. Fujimoto, H. Hoof, and D. Meger, "Addressing function approximation error in actor-critic methods," in *International Conference on Machine Learning*. PMLR, 2018, pp. 1587–1596.
- [7] V. Mnih, K. Kavukcuoglu, D. Silver, A. A. Rusu, J. Veness, M. G. Bellemare, A. Graves, M. Riedmiller, A. K. Fidjeland, G. Ostrovski *et al.*, "Human-level control through deep reinforcement learning," *nature*, vol. 518, no. 7540, pp. 529–533, 2015.
- [8] G. Dulac-Arnold, R. Evans, H. van Hasselt, P. Sunehag, T. Lillicrap, J. Hunt, T. Mann, T. Weber, T. Degris, and B. Coppin, "Deep reinforcement learning in large discrete action spaces," *arXiv preprint arXiv:1512.07679*, 2015.
- [9] "TS 38.331, NR; Radio Resource Control (RRC) protocol specification, Rel-16," 3GPP, Technical Specification, 2021.
- [10] F. B. Tesema, A. Awada, I. Viering, M. Simsek, and G. Fettweis, "Evaluation of context-aware mobility robustness optimization and multi-connectivity in intra-frequency 5G ultra dense networks," *IEEE Wireless Communications Letters*, vol. 5, no. 6, pp. 608–611, 2016.
- [11] D. Bertsekas, *Dynamic programming and optimal control: Volume I*. Athena scientific, 2012, vol. 1.
- [12] D. Silver, G. Lever, N. Heess, T. Degris, D. Wierstra, and M. Riedmiller, "Deterministic policy gradient algorithms," in *International conference on machine learning*. PMLR, 2014, pp. 387–395.
- [13] M. Muja and D. G. Lowe, "Scalable nearest neighbor algorithms for high dimensional data," *IEEE Trans. on pattern analysis and machine intelligence*, vol. 36, no. 11, pp. 2227–2240, 2014.
- [14] Y. Gao, W. Wang, J. Shi, and N. Yu, "Batch-constrained reinforcement learning for dynamic distribution network reconfiguration," *IEEE Trans. on Smart Grid*, vol. 11, no. 6, pp. 5357–5369, 2020.
- [15] A. Hyvärinen and P. Dayan, "Estimation of non-normalized statistical models by score matching," *Journal of Machine Learning Research*, vol. 6, no. 4, 2005.
- [16] S. Saremi, A. Mehrjou, B. Schölkopf, and A. Hyvärinen, "Deep energy estimator networks," *arXiv preprint arXiv:1805.08306*, 2018.
- [17] Network, NSN Self-Organizing, "Introducing the Nokia Siemens Networks SON Suite—an efficient, future-proof platform for SON," *White Paper, October*, 2009.
- [18] J. Meinila, P. Kyosti, L. Hentila, T. Jamsa, E. Suikkanen, E. Kunnari, and M. Narandzic, "D5. 3: WINNER+ final channel models," *Wireless World Initiative New Radio WINNER*, pp. 119–172, 2010.